Molecular Biology of the Cell
Vol. 12, 739–751, March 2001

The *Chlamydomonas PF6* Locus Encodes a Large Alanine/Proline-Rich Polypeptide That Is Required for Assembly of a Central Pair Projection and Regulates Flagellar Motility

Gerald Rupp,*† Eileen O'Toole,‡ and Mary E. Porter*§

*Department of Genetics, Cell Biology, and Development, University of Minnesota Medical School, Minneapolis, Minnesota 55455; and ‡Department of Molecular, Cellular, and Developmental Biology, University of Colorado at Boulder, Boulder, Colorado 80309

Submitted July 3, 2000, 2000; Revised November 29, 2000; Accepted January 16, 2000
Monitoring Editor: Thomas D. Pollard

Efficient motility of the eukaryotic flagellum requires precise temporal and spatial control of its constituent dynein motors. The central pair and its associated structures have been implicated as important members of a signal transduction cascade that ultimately regulates dynein arm activity. To identify central pair components involved in this process, we characterized a *Chlamydomonas* motility mutant (*pf6-2*) obtained by insertional mutagenesis. *pf6-2* flagella twitch ineffectively and lack the 1a projection on the C1 microtubule of the central pair. Transformation with constructs containing a full-length, wild-type copy of the *PF6* gene rescues the functional, structural, and biochemical defects associated with the *pf6* mutation. Sequence analysis indicates that the *PF6* gene encodes a large polypeptide that contains numerous alanine-rich, proline-rich, and basic domains and has limited homology to an expressed sequence tag derived from a human testis cDNA library. Biochemical analysis of an epitope-tagged PF6 construct demonstrates that the PF6 polypeptide is an axonemal component that cosediments at 12.6S with several other polypeptides. The PF6 protein appears to be an essential component required for assembly of some of these polypeptides into the C1-1a projection.

INTRODUCTION

Cilia and flagella are highly conserved structures found on diverse cell types, ranging from single-cell protozoa to multicellular tissues in humans, where they function to propel cells through a fluid environment or to transport fluid across a cell surface. Motile cilia are also found in the embryonic node (Sulik *et al.*, 1994; Bellomo *et al.*, 1996), where their motility appears to be critical for establishing the morphogenetic gradient that determines the left-right body axis in mammals (Nonaka *et al.*, 1998). Defects in the assembly or activity of cilia and flagella result in a variety of abnormalities, including defects in left-right axis asymmetry, infertility, and respiratory disease (Afzelius *et al.*, 1975; Afzelius, 1995; Supp *et al.*, 1999). Most motile cilia and flagella contain an axoneme that consists of nine outer doublet microtubules surrounding two central singlet microtubules. The outer doublets contain binding sites for the inner and outer dynein arms, the molecular motors that power axoneme motility (reviewed by Porter, 1996; King, 2000). The dynein arms on one outer doublet interact transiently with the adjacent doublet to generate the force for interdoublet microtubule sliding. Other structures within the axoneme constrain and coordinate the activity of the multiple dynein motors and thereby convert microtubule sliding into flagellar bending.

Both structural and genetic evidence indicate that the central pair microtubules and radial spokes play an important role in coordinating dynein activity. The two central pair microtubules are structurally asymmetric, and in several organisms, this apparatus has been shown to undergo clockwise rotation at a rate of approximately one turn per beat (reviewed by Omoto *et al.*, 1999). These observations led to the proposal that the central pair and its associated projections may act as a "distributor" that signals through the radial spokes to regulate the activity of the dynein arms. Consistent with this hypothesis, *Chlamydomonas* mutants that fail to assemble the central pair microtubules display paralyzed flagella, despite the ability of the dynein arms to

† Present address: Department of Anatomy, Southern Illinois University School of Medicine, Carbondale, IL 62901.
§ Corresponding author. E-mail address: mary-p@biosci.cbs.umn.edu.
Abbreviations used: EST, expressed sequence tag; FC-1, flanking clone 1; HA, hemagglutinin; kb, kilobase; PCR, polymerase chain reaction; PP1c, protein phosphatase, type 1 catalytic subunit; RT, reverse transcriptase; TAP, Tris-acetate phosphate.

drive microtubule sliding in disintegrating axonemes, albeit at a reduced rate (Witman *et al.*, 1978; Smith and Sale, 1992). Thus, the central pair microtubules appear to affect a control system that determines the pattern of dynein activity. Additional support for this hypothesis came from the characterization of bypass suppressors that restore partial motility to central pair and radial spoke defective strains without repairing the original missing structures (Huang *et al.*, 1982). The bypass mutations are thought to identify components in the signal transduction pathway between the central pair/radial spoke structures and the dynein arms. Characterization of the bypass mutations has identified defects in genes encoding components of the outer dynein arms (Huang *et al.*, 1982; Porter *et al.*, 1994; Rupp *et al.*, 1996), the inner dynein arms (Porter *et al.*, 1992; Myster *et al.*, 1997), and the dynein regulatory complex (Huang *et al.*, 1982; Piperno *et al.*, 1992). These and other studies suggest that the central pair microtubules regulate dynein arm activity through a signal transduction cascade that involves the radial spokes and the dynein regulatory complex.

Recent work in *Chlamydomonas* has demonstrated high levels of both structural and biochemical complexity within the central pair microtubules (Dutcher *et al.*, 1984; Mitchell and Sale, 1999). In *Chlamydomonas*, the C1 microtubule is associated with two long (18 nm) projections (1a and 1b) that repeat at 16-nm intervals and two smaller projections (1c and 1d) that repeat at 32-nm intervals. The C2 microtubule is associated with two 8-nm projections (2a and 2b) that repeat every 16 nm (Goodenough and Heuser, 1985) and one smaller density (2c). Mutations in at least four loci (*PF15, PF18, PF19,* and *PF20*) disrupt the assembly of the entire central pair apparatus and its constituent 25 polypeptides (Adams *et al.*, 1981; Dutcher *et al.*, 1984). Mutations at three other loci (*PF16*, *PF6*, and *CPC1*) result in only partial disruption of central pair structures (Dutcher *et al.*, 1984; Mitchell and Sale, 1999). At least 10 polypeptides are unique to the C1 microtubule, and seven are unique to the C2 microtubule (Dutcher *et al.*, 1984).

To identify central pair components involved in regulating flagellar motility, we used insertional mutagenesis procedures in *Chlamydomonas reinhardtii* (Tam and Lefebvre, 1993) to recover a new collection of "tagged" motility mutants (Myster *et al.*, 1997). Structural analysis of mutant axonemes identified one strain, 5B9, lacking the 1a projection on the C1 microtubule (Figure 1), a defect that resembles that previously described for *pf6-1* (Dutcher *et al.*, 1984; Mitchell and Sale, 1999). Genomic DNA flanking the site of plasmid insertion in 5B9 was recovered and used to obtain a full-length, wild-type copy of the *PF6* gene. Cotransformation with the wild-type gene fully rescued the motility and structural defects seen in both *pf6* strains. The predicted amino acid sequence of the *PF6* gene corresponds to a novel polypeptide of ~238 kDa that contains numerous proline-rich, alanine-rich, and basic domains. Localization of an epitope-tagged version of the *PF6* gene product within the axoneme indicates that the polypeptide appears to be an essential structural component required for the assembly of the 1a projection on the C1 microtubule.

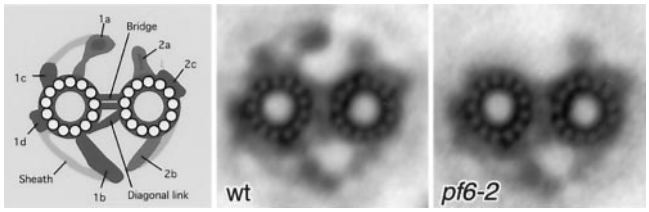

Figure 1. Central pair structure. (Left) Diagrammatic representation of the multiple projections associated with the central pair apparatus; redrawn from Mitchell and Sale (1999). The C1 microtubule (left) is associated with two 18-nm-long projections (1a and 1b) and two smaller projections (1c and 1d). Projections 1b and 1d appear to be linked by a thin sheath. The C2 microtubule (right) is associated with two 8-nm-long projections (2a and 2b) and one smaller projection (2c). The C1 and C2 microtubules appear to be linked by a two-membered bridge and a diagonal link that extends from the C2 microtubule to the C1 microtubule near the base of the C1–1b projection. (Middle) Image average of central pair structure from wild-type (wt) axonemes (n = 32). (Right) Image average of central pair structure from pf6-2 axonemes (n = 27). Note the absence of the 1a projection on the C1 microtubule.

MATERIALS AND METHODS

Cell Culture and Mutant Strains

All strains used in this study are listed in Table 1. Cells were maintained as vegetatively growing cultures on Tris-acetate phos-

Table 1. Strains used in this study

Strain	Structural defect	Motility phenotype	Reference
Wild type (137c)	None	Fast forward swimming	Harris, 1989
*nit1*Δ (A54e18)	None	Fast forward swimming	Nelson et al., 1994
pf6-1	Central pair projection	Twitchy	Dutcher et al., 1984
pf6-2	Central pair projection	Twitchy	This study
pf6-1 rescue	None	Fast forward swimming	This study
pf6-2 rescue	None	Fast forward swimming	This study
arg7	None	Fast forward swimming	Harris, 1989
arg2	None	Fast forward swimming	Harris, 1989
pf6-1 arg2	Central pair projection	Twitchy	This study
pf6-2 arg7	Central pair projection	Twitchy	This study
$\frac{pf6\text{-}1\,arg2}{pf6\text{-}2\,arg7}$	Central pair projection	Twitchy	This study

phate (TAP) media (Gorman and Levine, 1965) or TAP medium supplemented with 0.6 mg/ml L-arginine. The motility mutant 5B9 was generated by glass-bead–mediated transformation of the *nit*− strain A54e18 (*nit1*Δ *ac17 sr1*) with the *NIT1* gene as described by Myster *et al.* (1997).

Genetic and Phenotypic Analyses

Genetic analysis was performed using standard techniques (Levine and Ebersold, 1960; Harris, 1989). To determine whether the motility phenotype of 5B9 was linked to the *NIT1* plasmid used as a selectable marker, 5B9 was backcrossed to A54-B2 (*nit1*Δ *ac17 sr1*), and the resulting progeny were analyzed for their motility phenotypes and their ability to grow on selective media. Of 36 progeny obtained from 8 complete and 2 incomplete tetrads, 18 were found to be *nit*+ and unable to swim, whereas all 18 *nit*− strains had wild-type motility.

Recombination tests were performed by mating 5B9 to *pf6* and analyzing the motility phenotypes of the resultant tetrad progeny by light microscopy. Complementation tests were performed by constructing stable diploid cell lines using the complementing *arg*2 and *arg*7 markers (Ebersold, 1967). Assessment of motility phenotypes and measurements of swimming velocity were performed as previously described (Rupp *et al.*, 1996).

Nucleic Acid Analysis

Large-scale preparations of genomic DNA from wild-type and mutant strains were purified using CsCl gradients as described by Porter *et al.* (1996). A smaller scale, miniprep procedure (Newman *et al.*, 1990) was used to isolate DNA samples from tetrad progeny. Restriction enzyme digests, agarose gels, isolation of total RNA, preparation of cDNA, polymerase chain reaction (PCR) reactions, and Southern and Northern blots were performed as previously described (Porter *et al.*, 1996, 1999; Myster *et al.*, 1997).

Isolation of Genomic Sequence Flanking the NIT1 Plasmid

To identify genomic DNA flanking the site of the plasmid insertion, wild-type and *pf6-2* genomic DNA samples were analyzed on Southern blots, and a 2.8-kilobase (kb) *Bam*HI/*Cla*I fragment unique to *pf6-2* was identified by hybridization with a probe derived from the 3′-end of the *NIT1* gene. The 2.8-kb *Bam*HI/*Cla*I junction fragment was recovered by screening a size-fractionated mini-library with the *NIT1* probe as previously described (Smith and Lefebvre, 1996; Myster *et al.*, 1999; Perrone *et al.*, 2000). Plasmid DNA from two positive clones was purified using Wizard Maxi-prep kits (Promega, Madison, WI) according to the manufacturer's directions, digested with a variety of restriction enzymes, and probed with the *NIT1* plasmid to identify a 1.0-kb *Pvu*II fragment containing only *pf6-2* genomic DNA. Southern blot analysis of wild-type and *pf6-2* DNA confirmed that this fragment, designated flanking clone 1 (FC-1), was located close to the site of plasmid insertion.

Isolation of Genomic Clones and Sequence Analysis

A large insert, wild-type (21gr), genomic library constructed in λFIX II (Schnell and Lefebvre, 1993) was screened with FC-1 as previously described (Porter *et al.*, 1996; Myster *et al.*, 1997). Six overlapping phage clones were recovered and restriction mapped with the enzymes *Sac*I and *Not*I. Selected subclones were sequenced by primer walking at the DNA Sequencing Facility at Iowa State University (Ames, IA), and the resulting sequence data were analyzed using both MacVector 6.0 and the GCG suite of programs (Genetics Computer Group, Madison. WI).

Potential open reading frames were identified using the GCG program *CodonPreference* and a *Chlamydomonas* codon usage table (Myster *et al.* 1997) or the web-based programs GenScan (CCR-081.mit.edu/GENSCAN.html), and GeneMark (dixie.biology.gatech.edu/GeneMark/eukhmm.cgi). All splice junctions were confirmed by sequence analysis of reverse transcriptase (RT)-PCR products derived from the *PF6* transcript. The predicted amino acid sequence of the *PF6* gene was used to search for sequence homologies using Blast. Other sequence features were identified using the GCG programs Motifs and Coils.

Construction of Epitope-tagged Gene Construct

To ascertain whether the *PF6* gene product was a structural component of the axoneme, a modified gene containing a hemagglutinin (HA)-epitope was constructed using the CD-tagging technique described by Jarvik *et al.* (1996). The CD cassette contains an open reading frame that encodes the HA-epitope flanked on both sides by consensus sites for RNA splicing. When the CD cassette is inserted into a target intron of the host gene, the resulting construct contains two chimeric introns surrounding a new guest exon. To make an epitope-tagged *PF6* construct, the 20-kb *Xba*I insert contained within the rescuing phage clone, λL1a, was subcloned into the *Xba*I site of pBluescript II, resulting in the plasmid p5B9-X. A 10-kb *Acc*III/*Sal*I fragment containing the complete *PF6* transcription unit was further subcloned into pBluescript II digested with *Xma*I and *Sal*I, producing the plasmid p5B9-A/S. A 250-basepair fragment containing the HA-epitope tag was released from pCD-0 (kindly provided by J. Jarvik) with *Sma*I and then ligated into a unique *Sna*BI site in p5B9-A/S, yielding pSET-41. The pSET-41 construct contains a full-length copy of the *PF6* gene with an exon encoding the HA tag inserted into the eighth intron.

Transformation and Screening for Rescue of Motility Defect

To determine whether any of the recovered phage clones or *PF6* gene constructs could rescue the motility defects in the *pf6* mutants, *pf6 arg7* strains were cotransformed with pARG7.8 (containing a wild-type copy of the argininosuccinate lyase gene; Debuchy *et al.*, 1989) and the *PF6* clone being tested. After growth for 7–10 d on selective media, the motility phenotypes of the *arg*+ transformants were scored using a dissecting microscope. Transformants with apparent wild-type motility were grown in TAP media and reassayed by phase-contrast light microscopy to confirm their phenotype.

Fractionation of Flagella

Large-scale cultures (20 l) of vegetative cells for protein purification were grown in rich medium as described by Myster *et al.* (1997). Isolated axonemes were first extracted with a 0.6 M NaCl buffer and then re-extracted with a 0.2 M KI buffer to solubilize the C1 microtubule and associated structures (Mitchell and Sale, 1999). The KI extract was further fractionated by sucrose density gradient centrifugation (Porter *et al.*, 1992).

SDS-PAGE and Immunoblot Analysis

Protein samples were separated on either 6% polyacrylamide or 5–15% acrylamide, 0–2.4 M glycerol gradient gels using the Laemmli (1970) buffer system. Gels were stained directly with either Coomassie Brilliant Blue R-250 or silver (Wray *et al.*, 1981) or transferred to Immobilon-P (Millipore, Bedford, MA) as described by Myster *et al.* (1999). Protein transfer was assayed using Blot Fast-Stain (Chemicon, Temecula, CA). Western blots were probed with a high-affinity rat antibody directed against the HA-epitope (clone 3F10, Roche Molecular Biochemicals, Indianapolis, IN) and a donkey anti-rat secondary antibody labeled with alkaline phosphatase. Immunoreactive bands were detected using either colorimetric or chemilimunescent detection methods.

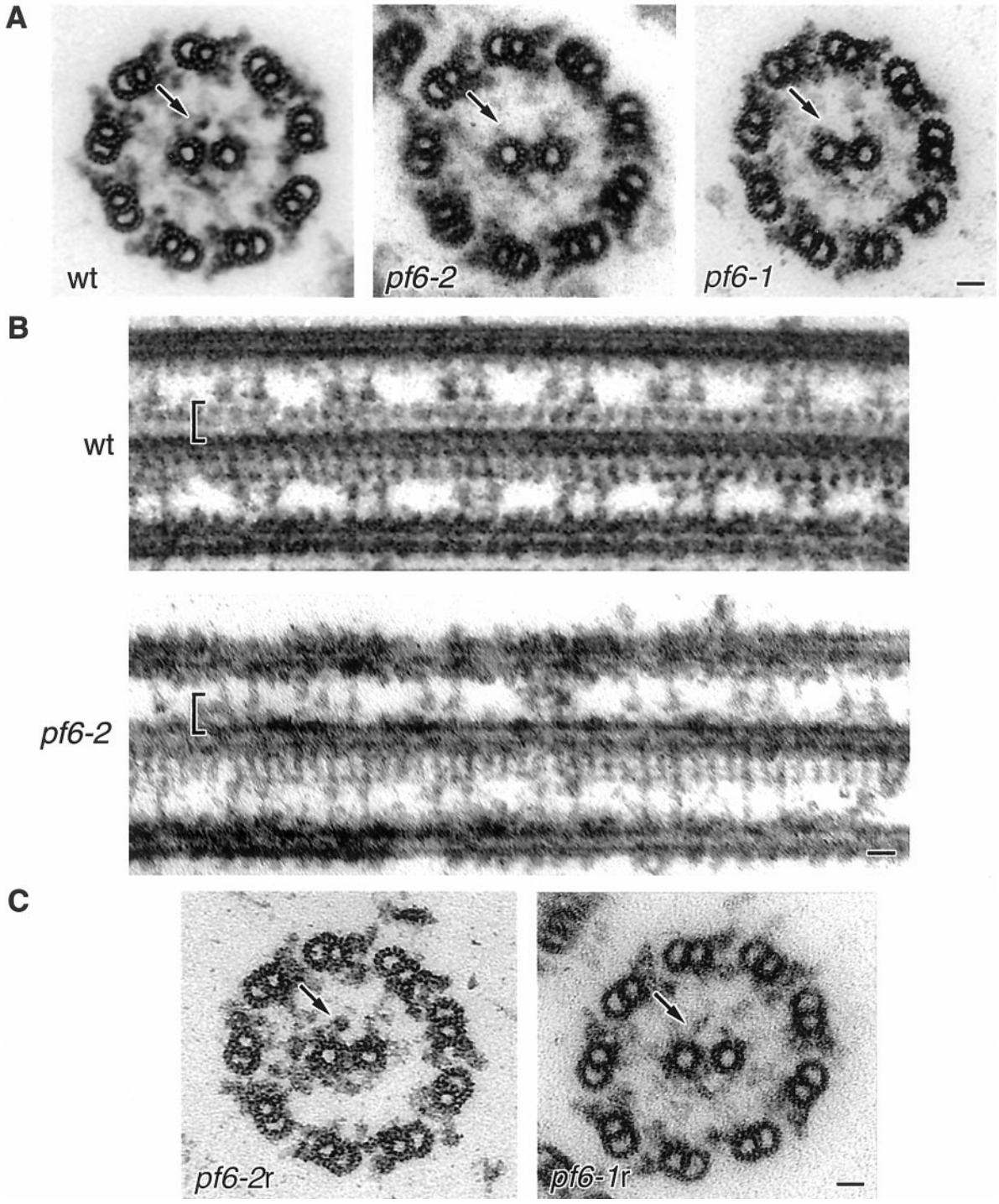

Figure 2. Electron microscopic analysis of axonemes from wild-type (wt) and mutant *Chlamydomonas* cells. (A) Transverse sections of flagellar axonemes reveal that the C1-1a projection present in wild-type samples is missing from *pf6-2* and *pf6-1* preparations (arrows). (B) Longitudinal images reveal two rows of projections repeating at precise 16-nm intervals in wild-type samples, but one row of projections is missing in the *pf6–2* axonemes (brackets). The observed central pair microtubule is identified as C1 based on the length of the remaining associated projections. (C) Rescue of the *pf6* mutant motility defect by transformation with a clone containing a full-length wild-type copy of the *PF6* gene is also accompanied by restoration of the C1-1a projection in both *pf6-2* and *pf6-1*, as observed in axoneme cross-sections (arrows). Bars, 25 nm.

Electron Microscopy and Image Analysis

Axonemes were prepared for electron microscopy as described by Porter *et al.* (1992). The methods for digitization and image averaging were as previously described (Mastronarde *et al.*, 1992; O'Toole *et al.*, 1995) with modifications described by Mitchell and Sale (1999).

Immunofluorescence

The *pf6-2* mutant and the epitope-tagged rescued strains were prepared for immunofluorescence using the protocol described by Sanders and Salisbury (1996). Samples were incubated in primary antisera directed against either α-tubulin (clone B-5-1-2, Sigma, St. Louis, MO) or the nine-amino acid HA-epitope (clone 3F10, Roche Molecular Biochemicals) overnight at 4°C in a humid chamber. After the samples were rinsed extensively, they were incubated in secondary antibodies conjugated with either Cy3 or Alexa-488. Control samples were either unlabeled or labeled with secondary antisera alone. Samples were imaged on a TE300 inverted fluorescence microscope (Nikon, Tokyo, Japan) equipped with a 60× oil objective. Images were collected using a C4742–95 digital camera (Hamamatsu, Bridgewater, NJ) and the Simple PCI software package (Compix, Cranberry Township, PA).

RESULTS

Recovery of a Tagged pf6 *Allele*

We screened a collection of motility mutants generated by insertional mutagenesis (Myster *et al.*, 1997) for cells with abnormal swimming behaviors to identify new mutations involved in the regulation of flagellar motility. One class of motility mutants contained strains that jiggled or twitched in place and made little or no forward progress, a phenotype typical of mutations that partially disrupt the assembly of the central pair apparatus (Dutcher *et al.*, 1984). Mutations that completely block central pair assembly usually result in paralyzed, rigid flagella (Witman *et al.*, 1978). Analysis of the transformants on genomic Southern blots identified one strain, 5B9, that contained only a single copy of the *NIT1* plasmid. 5B9 was backcrossed to a *nit*− strain with wild-type motility to verify that the aberrant motility phenotype of 5B9 was linked to the *NIT1* gene (see MATERIALS AND METHODS). Analysis of the resulting tetrad progeny confirmed that the mutant motility phenotype cosegregated with the *nit*+ phenotype (<5.6 cM apart).

To determine whether the 5B9 mutation was associated with morphological defects within the flagellar axoneme, demembranated axonemes were prepared for electron microscopy. Analysis of axoneme cross-sections revealed an obvious structural defect in the central pair apparatus. One of the two 18-nm projections associated with the C1 microtubule of the central pair was missing in the 5B9 axonemes (Figure 2A and Table 2). This missing structure corresponds to the 1a projection described by Mitchell and Sale (1999) and is more clearly seen in image averages of the central pair from wild-type and *pf6-2* axonemes shown in Figure 1. In addition, the 5B9 defect is strikingly similar to the structural defect previously observed in *pf6-1* axonemes (Figure 2A; Dutcher *et al.*, 1984). Analysis of longitudinal images (Figure 2B) confirmed that the structural defect in 5B9 affected one entire row of projections associated with the C1 microtubule of the central pair.

Recombination and complementation tests showed that the 5B9 mutation represents a new allele at the *PF6* locus. When 5B9 was mated to *pf6-1*, no recombinants were identified in 54 complete tetrads, demonstrating that the two mutations are very closely linked (<0.9 cM). Stable diploid cell lines obtained from a cross between 5B9 *arg7* and *pf6-1 arg2* also swam with the same aberrant motility phenotype as the two parent strains. Based on the close linkage and failure to complement, we have renamed the 5B9 strain *pf6-2*.

Table 2. Distribution of C1 associated projections

Number of projections on C1 microtubule	Number of cross-sectional images			
	Wild type	*pf6-1*[a]	*pf6-2*	*pf6-2* rescue
0	0	8	2	0
1	4	52	45	6
2	46	2	3	44
Total	50	62	50	50

[a] Data from Dutcher et al., 1984.

Recovery of the PF6 *Gene*

Southern blot analysis of *pf6-2* genomic DNA probed with the vector portion of the *NIT1* plasmid revealed that *pf6-2* contained a single *NIT1* plasmid that cosegregated with the mutation but that the vector sequence had been partially deleted during the insertion event. We therefore cloned genomic DNA flanking the site of plasmid insertion by constructing a size-fractionated, mini-library with *pf6-2* genomic DNA and screening this library with a probe from the *NIT1* gene (see MATERIALS AND METHODS and Figure 3A). The flanking clone, FC-1, was then used to screen a large insert, wild-type genomic phage library, and six overlapping phage clones spanning 32 kb of genomic DNA were recovered and restriction mapped (Figure 3). To test whether any of the phage clones contained a full-length copy of the *PF6* gene, three clones were analyzed for their ability to rescue the *pf6* mutant motility phenotype by cotransformation. Only one clone, λL1a, was able to restore wild-type swimming to either *pf6-1* or *pf6-2* cells (Figure 3C). The recovery of a wild-type swimming phenotype was accompanied by the reassembly of the C1-1a projection (Figure 2C and Table 2). The λK1a phage clone, which shares ~40% overlap with λL1a, failed to rescue the *pf6* motility defect, suggesting that the *PF6* gene must extend beyond the limits of this clone.

To define the boundaries of the *PF6* gene, selected restriction fragments were subcloned and used to probe Southern and Northern blots. Plasmid insertions into the nuclear genome of *Chlamydomonas* are often accompanied by deletions or rearrangements of the surrounding genomic region. However, Southern blot analysis of wild-type and *pf6-2* genomic DNA probed with the subclones shown in Figure 3B indicated that the *NIT1* plasmid inserted into a 0.6-kb *Sac*I restriction fragment without significant deletion or rearrangement of the surrounding region (Figure 3A). These results suggested that there was not a major deletion of the *PF6* transcription unit in *pf6-2*.

To identify the limits of the *PF6* transcription unit and the size of the *PF6* transcript, the *Sac*I subclones labeled A–E

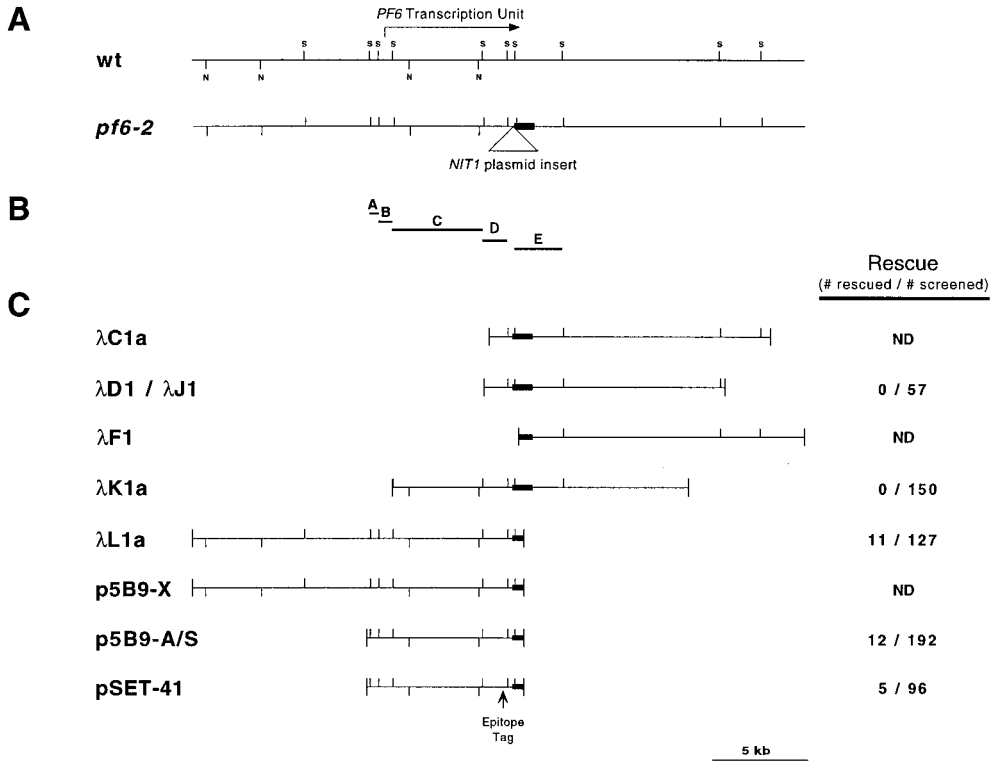

Figure 3. Recovery of the *PF6* transcription unit. (A) Partial restriction maps of the genomic DNA region containing the *PF6* transcription unit from wild-type (wt) and *pf6-2*. Also indicated on the diagram is the location of the NIT1 plasmid insertion in *pf6-2* and the position of the flanking clone FC-1 (black box) representing the *Pvu*II restriction fragment recovered from a size-fractionated mini-library. S, *Sac*I sites; N, *Not*I sites. (B) Selected *Sac*I fragments (A–E) that were used to map the boundaries of the plasmid insertion in *pf6-2* and determine the size of the *PF6* transcription unit. (C) Alignment of the six overlapping phage clones recovered with the flanking clone FC-1 (black boxes) and the three plasmid clones, derived from the λL1a insert, that contain the PF6 transcription unit. The plasmid pSET-41 contains an epitope-tagged *PF6* gene construct. Also indicated are the number of rescued strains observed by cotransformation with the selected clones.

(Figure 3B) were also hybridized to Northern blots loaded with total RNA isolated from wild-type, mutant, and rescued cells both before and 45 min after deflagellation. Deflagellation is known to induce up-regulation of transcripts that encode flagellar proteins (reviewed by Lefebvre and Rosenbaum, 1986). Probes B, C, and D identified a single transcript of ~7 kb that was highly up-regulated after deflagellation in wild-type cells (Figure 4). No transcripts were detected with probe A, whereas probe E only hybridized weakly to the 7-kb transcript recognized by probes B–D, suggesting that it contained only a small portion of the *PF6* transcription unit. The 7-kb transcript seen in deflagellated, wild-type samples was present at reduced levels in the original *pf6-1* mutant, completely absent in the insertional allele *pf6*-2, and restored after rescue with a full-length, wild-type copy of the *PF6* gene (Figure 4). Interestingly, the *pf6-2* mutant expressed two larger up-regulated transcripts that were not present in the wild-type sample. These most likely represent hybrid transcripts generated by insertion of the *NIT1* gene into the 3′-end of the *PF6* transcription unit (Figure 3A). Given the *pf6-2* mutant phenotype, the protein products encoded by these hybrid transcripts do not appear to be competent for assembly into the flagellar axoneme.

Characterization of the PF6 Gene and Gene Product

Sequence analysis from ~12 kb of genomic DNA containing the *PF6* gene indicated that the *PF6* transcription unit contains nine exons and eight introns spanning ~9.5 kb of genomic sequence (Figure 5A). A second gene bearing homology to the 39-kDa subunit of NADH ubiquinone oxidoreductase lies immediately upstream of the *PF6* transcription unit. The *PF6* gene is predicted to encode a 2301-amino acid polypeptide (Figure 6) with a calculated molecular mass of ~238 kDa and a predicted pI of 4.65. The predicted *PF6* amino acid sequence contains numerous proline-rich domains, an alanine-rich domain, two basic domains, and two predicted coiled-coil domains (Figure 5B). Database searches revealed limited homologies to other proteins containing proline-rich regions. However, recent searches have identified a more significant homology to a 3′-expressed sequence tag (EST) derived from a human testis cDNA library (Figure 7).

Location of the PF6 *Gene Product*

Previous biochemical characterization of *pf6-1* axonemes revealed the loss of three polypeptides of 20, 66, and 97 kDa, but none of these polypeptides appeared to be the *PF6* gene product (Dutcher *et al.*, 1984). Based on the predicted size of the *PF6* gene product (~238 kDa), we have confirmed the hypothesis that the *PF6* gene does not encode any of the three missing polypeptides previously identified. These results suggest that the *PF6* gene product might be either a structural component of the central pair that was previously difficult to resolve by SDS-PAGE or a factor required for assembly of the C1-1a projection that is extrinsic to the axoneme.

To determine whether the *PF6* gene encodes a central pair component required for assembly of the C1-1a projection, an epitope-tagged gene construct was used to rescue the *pf6* mutant phenotype. A single HA-epitope tag was inserted into the eighth intron of the *PF6* gene (Figures 3C and 5A). The resulting construct is predicted to encode an ~239-kDa

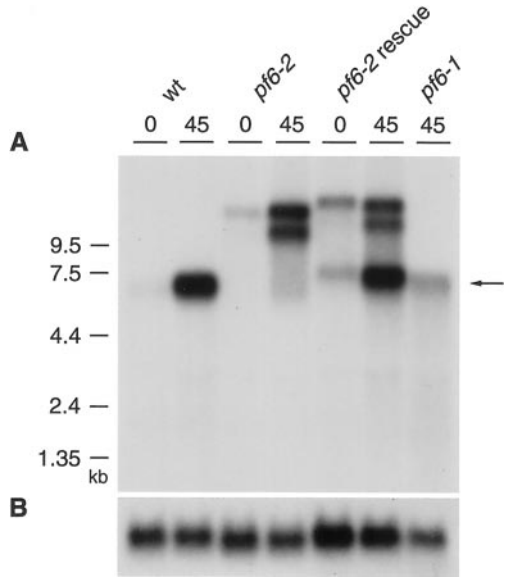

Figure 4. Expression of the *PF6* transcript. (A) Northern blot loaded with total RNA isolated from wild-type, *pf6* mutants, and a rescued *pf6* strain before (0) and forty-five (45) min after deflagellation. This blot was probed with an RT-PCR product from within probe C (Figure 3) and is representative of blots hybridized with probes B, C, and D. The ~7-kb *PF6* transcript is indicated (arrow). The slight upward shift in transcript migration in the *pf6-2* rescue lanes appears to result from differences in the loading of these lanes relative to the others. (B) The same Northern blot shown above was rehybridized with a probe for the *CRY1* gene, which encodes the ribosomal S14 protein subunit (Nelson et al., 1994), as a control for loading of the RNA samples.

polypeptide with the nine-amino acid HA-epitope tag inserted between residues 1910 and 1911 of the PF6 sequence (Figure 5B). Cotransformation with the epitope-tagged transgene rescues the aberrant motility phenotype of *pf6-2* cells as efficiently as the wild-type gene, demonstrating that the presence of the epitope tag does not interfere with the function of the PF6 protein (Figure 3C). Axoneme samples from wild-type, *pf6-1*, *pf6-2*, and rescued *pf6-2* strains were therefore analyzed on Western blots probed with an antibody directed against the nine-amino acid HA-epitope. As shown in Figure 8A, a single polypeptide that migrates with an apparent molecular mass slightly larger than 250 kDa is observed exclusively in the epitope-tagged rescued strain, indicating that the PF6 protein is a structural component of the isolated axoneme.

Mutant and rescued cells were labeled with antibodies directed against either α-tubulin or the HA-epitope to analyze the subcellular distribution of the PF6 protein. Indirect immunofluorescence of *pf6* mutant and *pf6* rescued cells with the tubulin antibody demonstrated that both strains assemble full-length flagella (Figure 8B, a and d). Staining with the HA antibody revealed that the tagged PF6 polypeptide is present along the entire length of the axoneme in the rescued strain (Figure 8B, e and f) and absent from *pf6-2* samples (Figure 8B, b). The cell body fluorescence seen in Figure 8B (b, e, and f) appears to result from autofluorescence, because a similar pattern was observed after treatment with secondary antibody alone (Figure 8B, c).

To examine whether the PF6 protein is part of a larger polypeptide complex associated with the C1 microtubule, axoneme extracts from both *pf6-2* and the rescued strain were analyzed by sucrose density gradient centrifugation and western blotting. Previous work had demonstrated that treatment with a 0.6 M NaCl buffer will solubilize the dynein arms and the C2 microtubule, but that the C1 microtubule is partially resistant to salt extraction (see figure 5 in Mitchell and Sale, 1999). However, the C1 microtubule is efficiently solubilized by treatment with 0.2 M KI (Mitchell and Sale, 1999). As shown in Figure 9A, 0.6 M NaCl treatment of isolated axonemes (lane 2) from the *pf6-2* rescued strain solubilized only a portion of the HA-tagged PF6 protein (compare supernatant in lane 3 to pellet in lane 4). However, subsequent extraction with 0.2 M KI effectively solubilized all of the remaining HA-tagged PF6 polypeptide (Figure 9A, lane 5), consistent with its proposed location in the C1 microtubule.

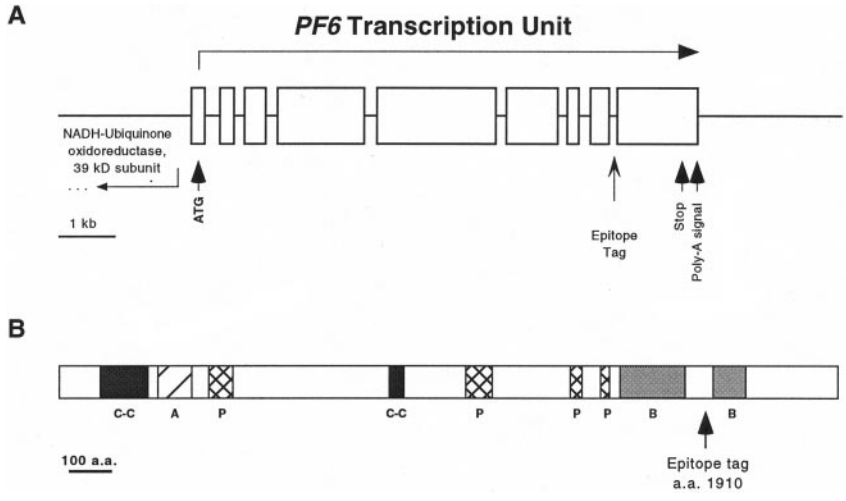

Figure 5. Structure of the *PF6* gene and polypeptide. (A) Diagram of the proposed intron-exon structure of the *PF6* transcription unit. Open rectangles indicate exons and solid lines indicate introns. The predicted translation start (ATG) and stop sites are indicated, as well as the putative polyadenylation signals (Poly-A). The location of the epitope tag inserted into intron 8 is marked. (B) Diagrammatic representation of the domain structure of the *PF6* gene product. Indicated are the location of proline-rich (P; cross-hatched boxes), alanine-rich (A; single-hatched boxes), basic (B; gray, shaded boxes), and probable coiled-coil (c-c; black boxes) domains and the location of the inserted epitope tag. a.a., amino acid.

```
        *         *         *         *         *         *         *         *         *
   1 MAPKPKKPEAAPPPPPEPSPDDNLPQDIKELTECPFEVTWKPVVSIVDYGVGADAKGIQATLKRKELARYIVLHEAVLRLDPATPLGQEAKAVLDAHIAA  100
        *         *         *         *         *         *         *         *         *
 101 GQGPETCTFGPELSSKLLADKFARDQLADWRVELHRRRTRLQAAQDDATAAAAGLTAAHEAVKAAGEALAAYHRGVEEEEARKAAQRAEEGEEEPPTPLD  200
        *         *         *         *         *         *         *         *         *
 201 DEEGAAPVEREAPAEEVALEQAKAAVVAAEVQVRETAETASRLAAVQNEPFVCYQTYILSGLTLSLASVRKALEEGTPLRGVLWAKAAAPAAPADGAAAA  300
        *         *         *         *         *         *         *         *         *
 301 PDAAAAAAAAAEPAPWYAAVKKAAQKALWEDVLAQLVPLEVQVPAYTPPPPPEAEPAKGKKPSSAKPTAAKGAKGAAAAAAAAVAAAAVEAPPAPPEDSP  400
        *         *         *         *         *         *         *         *         *
 401 GWDAVSEVLKTLAYNVRTYDEWRAKVKVYDASKYDEVPAPPPEPEPEAPPPPPPEPVLPPPPAAGAKTPSAKGGRTTPPAPPPPPPPPPEPEPEPTPPPP  500
        *         *         *         *         *         *         *         *         *
 501 PPAGPMPPPHNLGYYSALLDGVPLERVSVPLVMHALLEQVARNMASGEAGEDLTEAGGMAAAEMAALSALDGALSALDTELQEAVFAPPKPEAADYSLVC  600
        *         *         *         *         *         *         *         *         *
 601 EVDGLAAAAAGLTTGWVRAAPPRPESPTSHLDAAAAVAAEPSVLGAPASEASGGAGSVFGGASYGTGPEGLFTHSGTLDVEAVEAHMLRCMMLPGAQSFA  700
        *         *         *         *         *         *         *         *         *
 701 DARAAAGELAASGSFGMGTGLDALSKSLRRTALQAEAEALPVATIERYQLLQAAVDLLPPSAKLSHEDAILARHWHEPLDGPRLKQALAEAVTELPSMSS  800
        *         *         *         *         *         *         *         *         *
 801 VYYGPADSVVVACYAAENLRSTAADLPVAMNLSAFVRRAAAAAPGPVDLPAKVYKMAPELAAGVEAHQRTAFLYPQTACIVSAPMPAVTQEAAAESVPPG  900
        *         *         *         *         *         *         *         *         *
 901 VQTAATLASLAAEGSAPQPTGSLAISRGGVALRWREGSGAPADKAPGEGANDPSGAPLLLGTLPGGSVLSAFHVVDPAAAEAARLAEEEAARLAEEEEAK 1000
        *         *         *         *         *         *         *         *         *
1001 KKAEAEAAAAEEGSEDSGPAFKPMMSAAEALKAGNRGMFEDEDEDEDEDYGGGGDDLNTLLNKDKKPPPVTALQVTTPSGHLIRMTTDGQVLVAPADDPS 1100
        *         *         *         *         *         *         *         *         *
1101 LAPPLAPFRGVAVHGAPLPGADLAALRAPATPNAFRAVTRDGLLVSAARGAVARVLCPDGSVSERLDAVEGWLGPDGAAAARGWLRTALDGTRLREPDEG 1200
        *         *         *         *         *         *         *         *         *
1201 SKPKPPPTPPPEPESVAEPEPEVKGKGAKAGAKPASKDTLKKGKGKGKGGDDEPTPPPTPPPESRRPQPPPPPPPFTLELPAIGSATLTDPDTGARVTTRE 1300
        *         *         *         *         *         *         *         *         *
1301 DNVMVVAYPAGDVLVQDYDGTRITRAADGAWSVEMDGFAPILGSPAGLTISPCPGVTLSWDATTGVVTGTLPDGSAVLAAPHAAAFAPAGVQPPPLATLA 1400
        *         *         *         *         *         *         *         *         *
1401 SEPEALDEDEDDEDEDEDGNMRKKPKKEDPVAEAVAAANLLDELAANPDLSGIFLFDPRGGSCAFYESEQLRFFLLGPLARGAAQAAAKAKAGADDDEED 1500
        *         *         *         *         *         *         *         *         *
1501 DDDGGRPAKVFDVPKPYWPPPPPLLHIHIPELPPPPPPPPVVEEDEEEVKPAGGSRRPSLMDPDAGSDAEDEYGNSRRGTADGATGAGDGEEAAPPPPPR 1600
        *         *         *         *         *         *         *         *         *
1601 PPTPPPPEPVITYLPVAPHIKPRIFVIRNDGSGFEVLDTQLVSSYLAGRRQMAAESTARPGSAAKPGAAPGAAYGMAVELRREELHGGEEEGAVMHSVLV 1700
          *         *         *         *         *         *         *         *         *
1701 QVPQRPPALEPLPVGGAALLQRYRPHLEELMPAFKRLAQLVKPEPGAGLSTAQYLPRVMSYEPPVVRAAAPLPVLVYRELLELPALSGETIATIREVLAQ 1800
        *         *         *         *         *         *         *         *         *
1801 QARTEQTQAMMYAQAVPYSDPRPSETAAQDADVLAGILAMRSKPPIGRVRSVAAEVRRRRETSDAAAVAREQAARAREMATAINSEKEKRPWPVKVGPFD 1900
        *         *         *         *         *         *         *         *         *
1901 HTPKRPEEGMILPYFGSEEGILALENDPIIQQPINRRMLPPRLPPPAATPGAPSTYSPGVYVADRPAPPPGGSDLGAGAAAGVEYSSPSRLGATGASIMS 2000
        *         *         *         *         *         *         *         *         *
2001 RTGGAAGTDFAYPELAHSQILAQHTERAGPGPSLKSHAYDVYGQPRTLPPPVPRQHRADEAEAALNESYLRAEADAVRLGKTSSTQLIRAAGKALRQFAL 2100
        *         *         *         *         *         *         *         *         *
2101 TPSHLHLGTVPVGAVAHRTARLANVSTGAARFSVVRPELPLRAIYKPGPVAAGMEALITVEFVAEKVGDFVGEVTVKSELNVLTITVSAKVVPAQDGGDE 2200
        *         *         *         *         *         *         *         *         *
2201 AAVAAHDAGSSPARRGLESAGGGQLPPVTSGRKSASQSAVGSRLTSPLAGASRGASPAVGGHNVGGLDIPSLDETKTLNQVIHGDATGGAGAEEPAPEPA 2300

2301 P                                                                                                    2301
```

Figure 6. Predicted amino acid sequence of the PF6 gene product (GenBank accession AF327876).

Further fractionation of the 0.2 M KI extract by sucrose density gradient centrifugation indicated that the HA-tagged PF6 polypeptide sediments at ~12.6S with several additional polypeptides. The polypeptide composition of the gradient fractions is quite complex, but direct comparison to similar fractions from a *pf6-2* gradient indicates the presence of at least two polypeptides that cosediment with the HA-tagged PF6 polypeptide in the rescued sample but are missing in the *pf6-2* sample (Figure 9B, black dots). Two polypeptides present in the rescued sample and missing in the mutant sample were also observed (Figure 9B, open circles), but these bands were faint, and it was not possible to determine whether they cosedimented precisely with the HA-tagged PF6 protein in neighboring fractions. Interestingly, although the HA-tagged PF6 polypeptide was easily observed in the gradient fractions by Western blotting, it was also difficult to detect on silver stained gels in these partially purified samples (Figure 9B, arrow). Further characterization of the polypeptides associated with PF6 complex will therefore require the development of more extensive purification schemes.

```
PF6          2050  PPVPRQHRADEAEAALNESYLRAEADAVRLGKTSSTQLIRAAGKALRQFALTPSHLHLGTVPVGAVAHRTA  2120
Human cDNA      1  VKLPHYLLSSKPKSQP-LAKVQDSVGGKVNTSSVASAAINNAKSSLFGFHLLPSSVKFGVLKEGHTYATVV  70
                     :P:   :   :   : ::         : ::  I  A  :L  F L PS :: G :  G

PF6          2121  RLANVSTGAARFSVVR--PELPLRAIYKPGPVAAGMEALITVEFVAEKVGDFVGEVTVKSELNVLTITVSA  2189
Human cDNA     71  KLKNVGVDFCRFKVKQPPPSTGLKVTYKPGPVAAGMQTELNIELFATAVGEDGAKGSAHISHNIEIMTEHE  141
                    :L NV    :RF V :  P   L:  YKPGPVAAGM:: :::E  A  VG:    : :   N:  :T

PF6          2190  KVVPAQDGGDEAAVAAHDAGSSPARRGLESAGGGQLPPVTSGRKSASQSAVGSRLTSPL  2248
Human cDNA    142  VLFLPVEAT-VLTSSNYDKRPKDFPQGKENP----MVQRTSTIYSSTLGVFMSRKVSPH  195
                     :   :    : :  D       :G E      :   TS   S::     SR  SP
```

Figure 7. Clustal W alignment of the *PF6* gene product and the partial EST derived from a human testis cDNA library. The alignment in this region shows 41% similarity and 23% identity between the two sequences.

DISCUSSION

Composition and Structure of Central Pair Projections

The central pair microtubules and their associated projections play a significant role in the regulation of flagellar motility (Dutcher *et al.*, 1984; Smith and Lefebvre, 1997; Mitchell and Sale, 1999). The analysis of mutations that disrupt the central pair microtubules and/or its associated projections has further demonstrated that the polypeptide composition of the central apparatus is quite complex. In addition to tubulin, it contains >23 different polypeptides, at least 10 of which are associated with the C1 microtubule and 8 with the C2 microtubule (Adams *et al.*, 1981; Dutcher *et al.*, 1984). Thus far, only five of these polypeptides have been characterized at a molecular level. The *PF16* gene encodes an armadillo repeat protein implicated in stability of the C1 microtubule (Smith and Lefebvre, 1996). The *PF20* gene encodes a WD-repeat protein involved in cross-bridging the two central pair microtubules (Smith and Lefebvre, 1997). The *PF15* gene encodes the p80 subunit of the microtubule-severing protein katanin, which appears to be required for

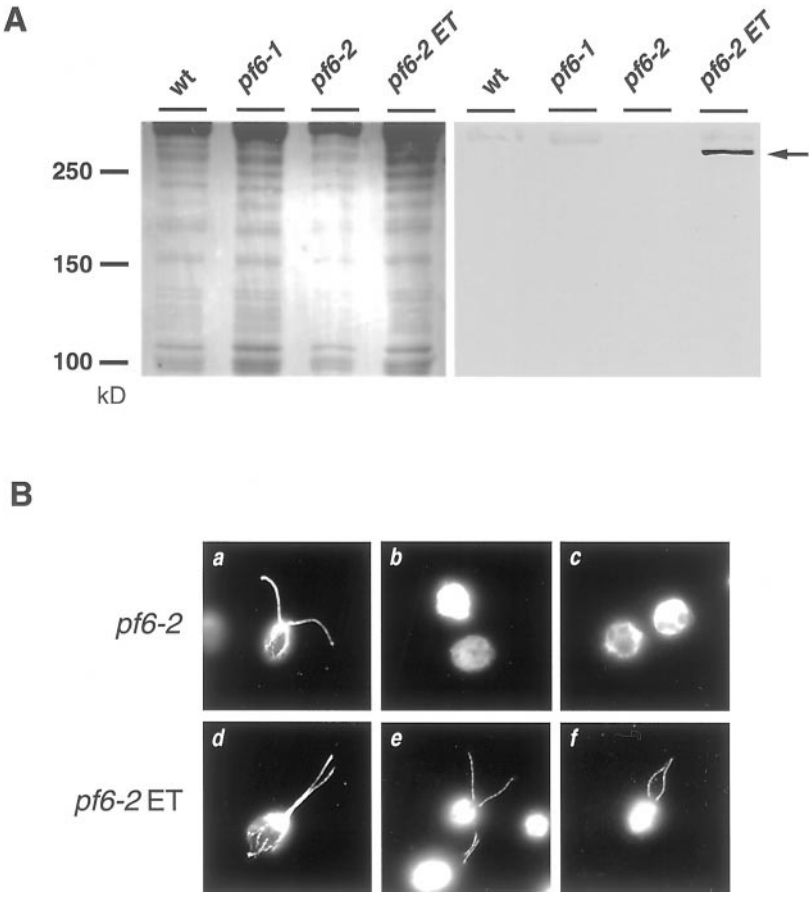

Figure 8. Localization of the *PF6* gene product. (A) Whole axonemes isolated from wild-type (wt), *pf6-1*, *pf6-2*, and a *pf6-2* strain rescued with the epitope-tagged *PF6* gene (pf6–2 ET) were separated on 6% acrylamide gels, blotted onto polyvinylidene difluoride, and stained with a reversible total protein stain (left) before immunolabeling with an antibody directed against the nine-amino acid HA epitope (right). The HA antibody recognized a single polypeptide present only in the *pf6-2* ET sample that migrates slightly larger than 250 kDa in this gel system (arrow). (B) Indirect immunofluorescent localization of the *PF6* gene product. *pf6-2* (a–c) and *pf6-2* ET (d–f) cells were labeled with antibodies against either α-tubulin (a and d) or the HA-epitope (b, e, and f). All of the recorded cells had flagella similar to those depicted in a and d. The tagged *PF6* polypeptide is present along the entire length of the axoneme in *pf6-2* ET cells (e and f). Control samples labeled with secondary antibody alone (c) demonstrate background cell body autofluorescence.

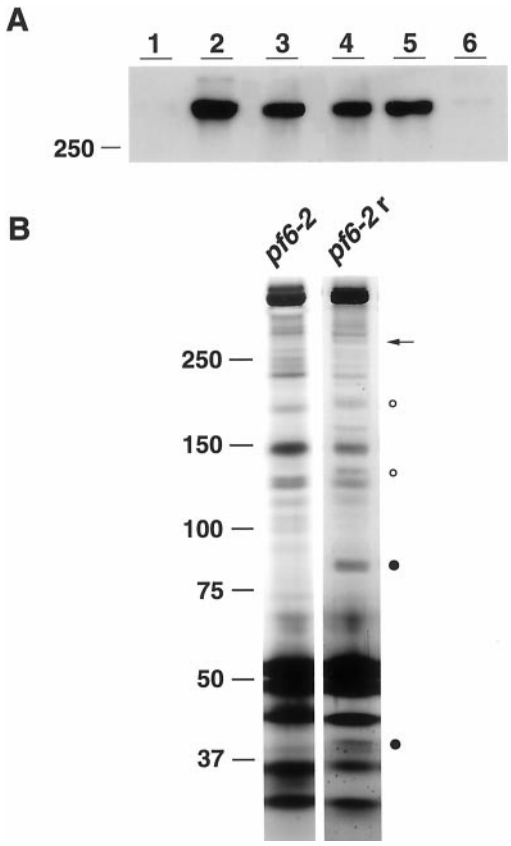

Figure 9. Polypeptides associated with the *PF6* gene product. (A) Isolated flagella from an epitope-tagged, *pf6-2* rescued strain were subjected to successive extractions and then analyzed on a Western blot probed with the anti-HA antibody. Lane 1, membrane plus matrix fraction; lane 2, whole axonemes; lane 3, 0.6 M NaCl supernatant; lane 4, 0.6 M NaCl pellet; lane 5, 0.2 M KI supernatant; lane 6, 0.2 M KI pellet. Note that only a portion of the epitope-tagged PF6 protein is solubilized by 0.6 M NaCl extraction (lane 3), whereas all of the remaining PF6 protein is released after treatment with 0.2 M KI (lane 5). (B) The 0.2 M KI extracts were subsequently fractionated by sucrose density gradients. The HA-tagged PF6 protein sedimented at ~12.6S, peaking in fraction 9. Silver-stained gels indicated that the polypeptide composition of these fractions was still quite crude, but several polypeptides observed in the rescued sample (*pf6*-2r) appear to be missing in the comparable fraction from the *pf6-2* gradient. The position of molecular weight standards is indicated. The arrow on the right indicates the approximate position of the HA-tagged *PF6* polypeptide seen on Western blots.

central pair assembly (Smith and Lefebvre, 1998). In addition, a type 1 protein phosphatase (Yang *et al.*, 2000) and an unusual kinesin-related protein (Bernstein *et al.*, 1994; Fox *et al.*, 1994; Johnson *et al.*, 1994) have been identified as central apparatus components. However, none of the polypeptides associated with the projection domains has been characterized. We have used insertional mutagenesis strategies to recover the *PF6* gene and to characterize the PF6 gene product.

pf6 mutant strains twitch in place as a result of flagella that beat slowly with a slightly abnormal waveform (Dutcher *et al.*, 1984; this study). Isolated *pf6* axonemes lack the 1a projection of the C1 microtubule, and previous biochemical analysis of *pf6-1* axonemes indicated that three polypeptides of 20, 66, and 97 kDa were missing. However, dikaryon rescue experiments suggested that the *pf6* defect did not reside in a gene encoding one of these three missing polypeptides but, rather, in another gene whose product was required for their proper assembly and/or targeting to the axoneme (Dutcher *et al.*, 1984). Consistent with this hypothesis, we found that the *PF6* gene encodes a large polypeptide (>238 kDa) that is targeted to the axoneme and appears to be required for assembly of polypeptides associated with the 1a projection of the C1 microtubule (Figures 1, 8, and 9). The PF6 protein is a highly acidic (pI 4.65), alanine-rich (18%) and proline-rich (12%) polypeptide that also contains two discrete, highly basic domains. These domains may be involved in microtubule binding but share no obvious homology with the basic domains previously identified in other axonemal proteins including, RSP3 (Diener *et al.*, 1993), PF16 (Smith and Lefebvre, 1996), and PF20 (Smith and Lefebvre, 1997). A better understanding of the functional significance of the various PF6 domains will require an in vivo analysis of constructs lacking specific domains.

Recent database searches with the PF6 sequence have revealed limited homology to an EST derived from a human testis cDNA library (Figure 7). Additional sequence information concerning the human cDNA will be needed to determine whether this is the human version of the *PF6* gene; however, its expression in the testis is consistent with a potential flagellar function. Interestingly, recent studies have demonstrated that several of the central pair polypeptides first characterized in *Chlamydomonas* have closely related (i.e., 60–70% identity) vertebrate homologues (Smith and Lefebvre, 1996, 1997; Neilson *et al.*, 1999; Sapiro *et al.*, 2000).

The large size of the PF6 protein (>238 kDa) and its sedimentation characteristics on sucrose density gradients (~12.6S) suggest that the PF6 polypeptide may serve as a molecular scaffold for the assembly of components associated with the 1a projection on the C1 microtubule. The *pf6* mutations result in the absence of the C1-1a projection (Figures 1 and 2) and the loss of two or more polypeptides that appear to cosediment with the PF6 protein (Figure 9B). Additional purification procedures will be needed to further characterize the components of the PF6 complex, to determine their relative stoichiometries and to relate them more directly to the central pair polypeptides previously described (Dutcher *et al.*, 1984; Mitchell and Sale, 1999). However, based on its sedimentation behavior, it is clear that the PF6 complex is distinct from the 16S complex of polypeptides associated with the C1-1b projection domain (Mitchell and Sale 1999). The C1 microtubule is also associated with a type 1 protein phosphatase (PP1c; Yang *et al.*, 2000) and a kinesin-related protein of ~105 kDa (Fox *et al.*, 1994). The location of these polypeptides within the substructure of the C1 microtubule is still unknown, but both appear to be present at wild-type levels in *pf6* and *cpc1* axonemes (Mitchell and Sale, 1999; Yang *et al.*, 2000; Rupp and Porter, unpublished observations). Whether the activity of either PP1c or the kinesin-related protein might be modified by the presence or absence of the projection domains is, however, an interesting question that remains to be determined (see below).

Possible Functions of the Central Pair Microtubules and Associated Projection Domains

In several organisms, the central pair appears to rotate approximately once per beat cycle (reviewed by Omoto *et al.*, 1999), forming transient interactions between the central pair projections and the radial spoke heads (Warner and Satir, 1974; Goodenough and Heuser, 1985). One current hypothesis is that a signal is transmitted to the radial spokes as the central pair projections periodically sweep past the radial spoke heads and that this signal is propagated to ultimately regulate dynein arm activity. A variety of kinases and phosphatases have recently been identified as tightly bound polypeptides located at discrete sites within the axoneme (Howard *et al.*, 1994; Roush and Sale, 1998; Yang and Sale, 2000; Yang *et al.*, 2000). Dynein arm activity may thus be regulated by the interaction of a network of kinases and phosphatases that are anchored at strategic locations within the central pair, radial spoke, and outer doublet structures in close proximity to their target proteins (reviewed by Porter and Sale, 2000).

The central pair apparatus therefore appears to play an important role in initiating a signal transduction cascade that ultimately regulates the pattern of dynein motor activity within the axoneme. Studies of reduced flagella (e.g., 3 + 0, 6 + 0) indicate that the simple propagation of bends does not require the presence of a central pair structure but that the motility of such organelles is primitive, displaying symmetric or helical waveforms (Schrevel and Besse, 1975; Prensier *et al.*, 1980). Central pair/radial spoke interactions may therefore be a refinement that is important for generating more complex, three-dimensional waveforms, and/or for higher order control that enables the cell to alter its waveform in response to external stimuli. For instance, wild-type *Chlamydomonas* cells can switch from an asymmetric (ciliary) beat pattern to a symmetric (flagellar) beat pattern in response to elevated calcium levels, and the central pair appears to be required for this conversion at physiological ATP levels (Hosokawa and Miki-Noumura, 1987). Central pair mutants can be induced to produce asymmetric waveforms under altered nucleotide or buffer conditions (Omoto *et al.*, 1996; Yagi and Kamiya, 2000). Yet, a great majority of motile axonemes possess a central apparatus, and most central pair defective mutants are paralyzed under physiological conditions (Witman *et al.*, 1978; Afzelius, 1985), consistent with an essential role in regulating motility.

Additional evidence for the involvement of the central pair in regulating bend symmetry has been provided from recent work with sea urchin sperm. Reactivated sea urchin sperm flagella switch from a symmetric to asymmetric waveform as a result of alterations in calcium concentration (Bannai *et al.*, 2000). This change in bend symmetry is apparently mediated by rotatable components within the axoneme (e.g., the central pair) and is the product of decreases in both microtubule-sliding velocity and reverse bend angle. Because only reverse bend curvature appears to be affected, it is possible that the "rotatable component" functions asymmetrically, such that only a specific domain (such as a central pair projection) regulates microtubule sliding that leads to reverse bend formation.

The asymmetry of the different central pair projections could therefore provide a precise control mechanism for a varied array of bending patterns under different conditions. Each central pair projection could have a unique role in the control of axoneme motility, possibly through associations with different regulatory enzymes. For example, *pf6* cells (lacking the 1a projection) swim poorly and their flagella beat slowly (Dutcher *et al.*, 1984; this report). In contrast, *cpc1* cells (lacking the 1b projection) swim fairly well, and their flagella beat with a wild-type waveform but at a reduced frequency (Mitchell and Sale, 1999). These differences in motility phenotypes suggest that one projection domain may be involved in regulating waveform, whereas the other domain may regulate beat frequency. Given the localization of PP1c within the C1 microtubule (Yang *et al.*, 2000), it is also possible that interactions between the central pair projections and the radial spoke heads could be altered based on the phosphorylation of key central pair polypeptides. The challenge for the future will be to identify additional polypeptides that are unique to each central pair structure and to determine their role in the signal transduction cascade that ultimately regulates dynein activity. Such studies may also provide insights into the regulation of other molecular motors.

ACKNOWLEDGMENTS

We thank other members of the Porter laboratory for their support and advice during this project, especially Raqual Bower and Cathy Perrone. We are also grateful to the members of the laboratories of Pete Lefebvre, Carolyn Silflow, and Dick Linck for their helpful suggestions. We extend special thanks to John Jarvik for kindly supplying plasmids containing the CD cassettes used for epitope tagging and Darryl Kruegger for assistance with electron microscopy. This work was supported by a grant from the National Institute of General Medical Sciences (GM-55667) to M.E. Porter. G. Rupp was supported in part by a National Institutes of Health postdoctoral fellowship (F32-GM17902) and a research training grant from the National Science Foundation for Interdisciplinary Studies on the Cytoskeleton (DIR-9113444). E. O'Toole was supported by a National Institutes of Health Biotechnology Resource grant (RR-00592) to J.R. McIntosh.

REFERENCES

Adams, G.M.W., Huang, B., Piperno, G., and Luck, D.J.L. (1981). Central-pair microtubular complex of *Chlamydomonas* flagella: polypeptide composition as revealed by analysis of mutants. J. Cell Biol. *91*, 69–76.

Afzelius, B.A. (1985). The immotile-cilia syndrome: a microtubule-associated defect. CRC Crit. Rev. Biochem. *19*, 63–87.

Afzelius, B.A. (1995). Role of cilia in human health. Cell Motil. Cytoskeleton *32*, 95–97.

Afzelius, B.A., Eliasson, R., Johnse, O., and Lindholmer, C. (1975). Lack of dynein arms in immotile human spermatozoa. J. Cell Biol. *66*, 225–232.

Bannai, H., Yoshimura, M., Takahashi, K., and Shingyoji, C. (2000). Calcium regulation of microtubule sliding in reactivated sea urchin sperm flagella. J. Cell Sci. *113*, 831–839.

Bellomo, D., Lander, A., Harragan, I., and Brown, N.A. (1996). Cell proliferation in mammalian gastrulation: the ventral node and notochord are relatively quiescent. Dev. Dyn. *205*, 471–485.

Bernstein, M., Beech, P.L., Katz, S.G., and Rosenbaum, J.L. (1994). A new kinesin-like protein (Klp1) localized to a single microtubule of the *Chlamydomonas* flagellum. J. Cell Biol. *125*, 1313–1326.

Debuchy, R., Purton, S., and Rochaix, J.-D. (1989). The arginosuccinate lyase gene of *Chlamydomonas reinhardtii*: an important tool for nuclear transformation and for correlating the genetic and molecular maps of the ARG7 locus. EMBO J. *8*, 2803–2809.

Diener, D.O., Ang, L.H., and Rosenbaum, J.L. (1993). Assembly of flagellar radial spoke proteins in *Chlamydomonas:* identification of the axoneme binding domain of radial spoke protein 3. J. Cell Biol. *123*, 183–190.

Dutcher, S.K., Huang, B., and Luck, D.J.L. (1984). Genetic dissection of the central pair microtubules of the flagella of *Chlamydomonas reinhardtii*. J. Cell Biol. *98*, 229–236.

Ebersold, W.T. (1967). *Chlamydomonas reinhardtii*: heterozygous diploid strains. Science *157*, 446–449.

Fox, L.A., Sawin, K.E., and Sale, W.S. (1994). Kinesin-related proteins in eukaryotic flagella. J. Cell Sci. *107*, 1545–1550.

Goodenough, U.W., and Heuser, J.E. (1985). Substructure of inner dynein arms, radial spokes, and the central pair/projection complex of cilia and flagella. J. Cell Biol. *100*, 2008–2018.

Gorman, D.S., and Levine, R.P. (1965). Cytochrome f and plastocyanin: their sequence in the photosynthetic electron transport chain of *Chlamydomonas reinhardtii*. Proc. Natl. Acad. Sci. USA *54*, 1665–1669.

Harris, E. (1989). The *Chlamydomonas* Sourcebook, San Diego, CA: Academic Press.

Hosokawa, Y., and Miki-Noumura, T. (1987). Bending motion of *Chlamydomonas* axonemes after extrustion of central-pair microtubules. J. Cell Biol. *105*, 1297–1302.

Howard, D.R., Habermacher, G., Glass, D.B., Smith, E.F., and Sale, W.S. (1994). Regulation of *Chlamydomonas* flagellar dynein by an axonemal protein kinase. J. Cell Biol. *127*, 1683–1692.

Huang, B., Ramanis, Z., and Luck, D.J. (1982). Suppressor mutations in *Chlamydomonas* reveal a regulatory mechanism for flagellar function. Cell *28*, 115–125.

Jarvik, J.W., Adler, S.A., Telmer, C.A., Subramaniam, V., and Lopez, A.J. (1996). CD-tagging: a new approach to gene and protein discovery and analysis. Biotechniques *20*, 896–904.

Johnson, K.A., Haas, M.A., and Rosenbaum, J.L. (1994). Localization of a kinesin-related protein to the central pair apparatus of the *Chlamydomonas reinhardtii* flagellum. J. Cell Sci. *107*, 1551–1556.

King, S.M. (2000). The dynein microtubule motor. Biochim. Biophys. Acta *1496*, 60–75.

Laemmli, U.K. (1970). Cleavage of structural proteins during the assembly of the head of bacteriophage T4. Nature *227*, 680–685.

Lefebvre, P.A., and Rosenbaum, J.L. (1986). Regulation of the synthesis and assembly of ciliary and flagella proteins during regeneration. Annu. Rev. Cell Biol. *2*, 517–546.

Levine, R.P., and Ebersold, W.T. (1960). The genetics and cytology of *Chlamydomonas.* Annu. Rev. Microbiol. *14*, 197–216.

Lewin, R.A. (1954). Mutants of *C. moewusii* with impaired motility. J. Gen. Microbiol. *11*, 358–363.

Mastronarde, D.N., O'Toole, E.T., McDonald, K.L., McIntosh, J.R., and Porter, M.E. (1992). Arrangement of inner dynein arms in wild-type and mutant flagella of *Chlamydomonas.* J. Cell Biol. *118*, 1145–1162.

Mitchell, D.R., and Sale, W.S. (1999). Characterization of a *Chlamydomonas* insertional mutant that disrupts flagellar central pair microtubule-associated structures. J. Cell Biol. *144*, 293–304.

Myster, S.H., Knott, J.A., O'Toole, E., and Porter, M.E. (1997). The *Chlamydomonas Dhc1* gene encodes a dynein heavy chain subunit required for assembly of the I1 inner arm complex. Mol. Biol. Cell *8*, 607–620.

Myster, S.H., Knott, J.A., Wysocki, K.M., O'Toole, E., and Porter, M.E. (1999). Domains in the 1α dynein heavy chain required for inner arm assembly and flagellar motility in *Chlamydomonas*. J. Cell Biol. *146*, 801–818.

Neilson, L.I., Schneider, P.A., Van Deerlin, P.G., Kiriakidou, M., Driscoll, D.A., Pellegrini, M.C., Millinder, S., Yamamoto, K.Y., French, C.K., and Strauss, J.F. (1999). cDNA cloning and characterization of a human sperm antigen (SPAG6) with homology to the product of the *Chlamydomonas* PF16 locus. Genomics *60*, 272–280.

Nelson, J.A.E., Savereide, P.B., and Lefebvre, P.A. (1994). The Cry1 gene in *Chlamydomonas reinhardtii*: structure and use as a dominant selectable marker for nuclear transformation. Mol. Cell Biol. *14*, 4011–4019.

Newman, S.M., Boynton, J.E., Gillham, N.W., Randolph-Anderson, B.W., Johnson, A.M., and Harris, E.H. (1990). Transformation of the chloroplast ribosomal RNA genes in *Chlamydomonas*: molecular and genetic characterization of integration events. Genetics *126*, 875–888.

Nonaka, S., Tanaka, Y., Okada, Y., Takeda, S., Harada, A., Kanai, Y., Kido, M., and Hirokawa, N. (1998). Randomization of left-right asymmetry due to loss of nodal cilia generating leftward flow of extraembryonic fluid in mice lacking KIF3B motor protein. Cell *95*, 829–837.

Omoto, C.K., Gibbons, I.R., Kamiya, R., Shingyoji, C., Takahashi, K., and Witman, G.B. (1999). Rotation of the central pair microtubules in eukaryotic flagella. Mol. Biol. Cell *10*, 1–4.

Omoto, C.K., Yagi, T., Kurimoto, E., and Kamiya, R. (1996). The ability of paralyzed flagella mutants of *Chlamydomonas* to move. Cell Motil. Cytoskeleton *33*, 88–94.

O'Toole, E., Mastronarde, D., McIntosh, J.R., and Porter, M.E. (1995). Computer-assisted image analysis of flagellar mutants. Methods Cell Biol. *47*, 183–191.

Perrone, C.A., Myster, S.H., Bower, R., O'Toole, E., and Porter, M.E. (2000). Insights into the structural organization of the I1 inner arm dynein from a domain analysis of the 1 β dynein heavy chain. Mol. Biol. Cell *11*, 2297–2313.

Piperno, G., Mead, K., and Shestak, W. (1992). The inner dynein arms I2 interact with a "dynein regulatory complex" in *Chlamydomonas* flagella J. Cell Biol. *118*, 1455–1463.

Porter, M.E. (1996). Axonemal dyneins: assembly, organization, and regulation. Curr. Opin. Cell Biol. *8*, 10–17.

Porter, M.E., Bower, R., Knott, J.A., Byrd, P., and Dentler, W. (1999). Cytoplasmic dynein heavy chain 1b is required for flagellar assembly in *Chlamydomonas*. Mol. Biol. Cell *10*, 693–712.

Porter, M.E., Knott, J.A., Gardner, L.C., Mitchell, D.K., and Dutcher, S.K. (1994). Mutations in the *SUP-PF-1* locus of *Chlamydomonas reinhardtii* identify a regulatory domain in the β-dynein heavy chain. J. Cell Biol. *126*, 1495–1507.

Porter, M.E., Knott, J.A., Myster, S.H., and Farlow, S.J. (1996). The dynein gene family in *Chlamydomonas reinhardtii*. Genetics *144*, 569–585.

Porter, M.E., Power, J., and Dutcher, S.K. (1992). Extragenic suppressors of paralyzed flagellar mutations in *Chlamydomonas reinhardtii* identify loci that alter the inner dynein arms. J. Cell Biol. *118*, 1163–1176.

Porter, M.E., and Sale, W.S. (2000). The 9 + 2 axonemal scaffold anchors multiple inner arm dyneins and a network of kinases and phosphatases that control motility. J. Cell Biol. *151*, F37–F42.

Prensier, G., Vivier, E., Goldstein, S.F., and Schrevel, J. (1980). Motile flagellum with a "3 + 0" ultrastructure. Science *207*, 1493–1494.

Roush, A.M., and Sale, W.S. (1998). A-kinase anchoring proteins (AkAPs) are localized to the central pair and radial spokes in flagellar axonemes. Mol. Biol. Cell *9,* 397a.

Rupp, G., O'Toole, E., Gardner, L.C., Mitchell, B.F., and Porter, M.E. (1996). The sup-pf-2 mutations of *Chlamydomonas* alter the activity of the outer dynein arms by modification of the γ-dynein heavy chain. J. Cell Biol. *135*, 1853–1865.

Sanders, M.A., and Salisbury, J.L. (1996). Immunofluorescence microscopy of cilia and flagella. Methods Cell Biol. *47*, 116–123.

Sapiro, R., Tarantino, L.M., Velasquez, F., Kiriakidou, M., Hecht, N.B., Bucan, M., and Strauss J.F. III. (2000). Sperm antigen 6 is the murine homologue of the *Chlamydomonas reinhardtii* central apparatus protein encoded by the *PF16* locus. Biol. Reprod. *62*, 511–518.

Schnell, R.A., and Lefebvre, P.A. (1993). Isolation of the *Chlamydomonas* regulatory gene NIT2 by transposon tagging. Genetics *134*, 737–747.

Schrevel, J., and Besse, C. (1975). Un type flagellaire fonctionnel de base 6 + 0. J. Cell Biol. *66*, 492–507.

Smith, E.F., and Lefebvre, P.A. (1996). The *PF*16 gene product contains armadillo repeats and localizes to a single microtubule of the central apparatus in *Chlamydomonas* flagella. J. Cell Biol. *132*, 359–370.

Smith, E.F., and Lefebvre, P.A. (1997). The role of central apparatus components in flagellar motility and microtubule assembly. Cell Motil. Cytoskeleton *38*, 1–8.

Smith, E., and Lefebvre, P. (1998). PF15 is required for central microtubule assembly and is homologous to katanin p80. Mol. Biol. Cell *9*, 278a.

Smith, E.F., and Sale, W.S. (1992). Structural and functional reconstitution of inner dynein arms in *Chlamydomonas* flagellar axonemes. J. Cell Biol. *117*, 573–581.

Sulik, K., Dehart, D.B., Iangaki, T., Carson, J.L., Vrablic, T., Gesteland, K., and Schoenwolf, G.C. (1994). Morphogenesis of the murine node and notochordal plate. Dev. Dyn. *201*, 260–278.

Supp, D.M., Brueckner, M., Kuehn, M.R., Witte, D.P., Lowe, L.A., McGrath, J., Corrales, J., and Potter, S.S. (1999). Targeted deletion of the ATP binding domain of left-right dynein confirms its role in specifying development of left-right asymmetries. Development *126*, 5495–5504.

Tam, L., and Lefebvre, P.A. (1993). Cloning of flagellar genes in *Chlamydomonas reinhardtii* by DNA insertional mutagenesis. Genetics *135*, 375–384.

Warner, F.D., and Satir, P. (1974). The structural basis of ciliary bend formation: radial spoke positional changes accompanying microtubule sliding. J. Cell Biol. *63*, 35–63.

Witman, G.B., Plummer, J., and Sander, G. (1978). *Chlamydomonas* flagellar mutants lacking radial spokes and central tubules: structure, composition, and function of specific axonemal components. J. Cell Biol. *76*, 729–747.

Wray, W., Boulikas, T., Wray, V.P., and Hancock, R. (1981). Silver staining of proteins in polyacrylamide gels. Anal. Biochem. *118*, 197–203.

Yagi, T., and Kamiya, R. (2000). vigorous beating of *Chlamydomoras* axonemes lacking central pair/radial spoke structures in the presence of salts and organic compounds. Cell Motil. Cytoskeleton *46*, 190–199.

Yang, P., Fox, L., Colbran, R.J., and Sale, W.S. (2000). Protein phosphatases PP1 and PP2A are located in distinct positions in the *Chlamydomonas* flagellar axoneme. J. Cell Sci. *113*, 91–102.

Yang, P., and Sale, W.S. (2000). Casein kinase I is anchored on axonemal doublet microtubules and regulates flagellar dynein phosphorylation and activity. J. Biol. Chem. *275*, 18905–18912.